

## Dielectronic satellite spectra of hydrogenlike chromium

K. R. Karim and C. P. Bhalla

*Department of Physics, Kansas State University, Manhattan, Kansas 66506*

(Received 28 July 1986)

Calculations of atomic parameters for dielectronic satellite lines of hydrogenlike chromium have been performed in the intermediate-coupling scheme with the inclusion of effects of configuration interaction. The doubly excited intermediate resonance states considered are  $|2l n l' SLJ\rangle$ ,  $n=2, 3$ , and 4 with all allowed values of  $l$  and  $l'$ . The Hartree-Fock-Slater atomic model is used to calculate transition rates. X-ray and Auger transition energies are corrected for relativistic effects. Radiative and radiationless transition rates, fluorescence yields, nonradiative branching ratio, and lifetime of these doubly excited states are reported. For the wavelengths of a few strong satellite lines, effects of self-energy and vacuum polarization are included in our calculation. Dielectronic recombination rate coefficients are presented as a function of electron temperature.

## I. INTRODUCTION

In low-density high-temperature plasmas, the dielectronic recombination is the dominant mechanism for producing doubly excited heliumlike states. A hydrogenlike ion in the ground state captures a free electron with an excitation of the core electron resulting in a doubly excited heliumlike ion of configuration  $nlnl'$ . Radiative transitions ( $1s-2p$ ) from such states produces satellite lines which appear on the long-wavelength side of the Lyman series. High-resolution x-ray spectra from hydrogenlike ions together with dielectronic satellite lines from doubly excited heliumlike states have been obtained in tokamak discharges,<sup>1-3</sup> solar active region and flares,<sup>4-10</sup> and laser-induced fusion devices.<sup>11-14</sup> These measurements as well as the observation of Li-like satellite lines<sup>15,16</sup> have been recognized as a potential diagnostic for the study of high-temperature and low-density plasmas.

Impurity atoms may enter the plasma as a result of plasma-wall interaction or they may be injected on purpose. The commonly used steel limiter in tokamaks contains Fe, Cr, Ti, and Ni. Recently Bitter *et al.*<sup>1</sup> have analyzed their high-resolution x-ray spectrum of doubly excited heliumlike titanium at TFTR (Tokamak Fusion Test Reactor, Princeton) with theoretical results obtained with the  $Z$ -expansion technique,<sup>17</sup> and with the Thomas-Fermi model. The dielectronic satellite spectra of H- and He-like systems of other elements that are to be investigated for diagnostics of the TFTR tokamak are Fe, Cr, and Ni.<sup>18,19</sup> Chromium and molybdenum have been found to be the dominant high- $Z$  contaminants in the high- $Z$  limiter Doublet III plasmas.<sup>20</sup> At TEXT (Texas Experimental Tokamak) spectra from Cr XVI-Cr XX have been recorded.<sup>21</sup> X-ray spectra of resonance, intercombination, and dielectronic satellite lines from heliumlike chromium have long been observed<sup>22</sup> at TFR (Tokamak de Fontenay-aux-Roses).

Calculations of the atomic parameters for the states of doubly excited heliumlike electron configuration  $nlnl'$  have been performed<sup>6,8,10</sup> for  $Z=12, 20$ , and 26 with  $n=2$ ,  $n'$  up to 5 using the multiconfiguration Thomas-Fermi (TF) atomic model.<sup>23</sup> Vainshtein and Safronova<sup>17</sup>

have employed the  $Z$ -expansion technique in their extensive calculations which are restricted to  $2l2l'$  configurations. Bitter *et al.*<sup>1</sup> list the result of both calculations for  $Z=22$  and significant differences were found in many cases in particular for  $n>2$  configurations.

We have completed new calculations for the states of  $nlnl'$  configurations with the Hartree-Fock-Slater (HFS) atomic model for Ne,<sup>24</sup> Mg, Si, Ar, Ca, Ti, Fe, Cr, and Ni. We report in the paper on our calculations of atomic parameters needed for the dielectronic spectra of hydrogenlike chromium and the total dielectronic recombination rates versus electron temperature. Section II contains theoretical considerations, followed by calculational procedure in Sec. III. Results and discussion are presented in Sec. IV.

## II. THEORY

## A. Dielectronic recombination rate coefficients

In the dielectronic recombination process<sup>25</sup> a free electron is captured by an ion initially in the ground state with the simultaneous excitation of one of the electron of the ion, and the resulting autoionizing state  $|s\rangle$  emits a photon leading to a final state  $|f\rangle$  that cannot autoionize.

For low-density plasmas, the intensity of the dielectronic satellite line,  $I_d(s-f)$  is given by

$$I_d(s-f) = n_e n_1 \alpha_d(s-f), \quad (1a)$$

where

$$\alpha_d(s-f) = \frac{1}{2} \left[ \frac{2\pi\hbar^2}{mkT_e} \right]^{3/2} F_2^*(s-f) \exp(-E_s/kT_e), \quad (1b)$$

$$F_2^*(s-f) \equiv (g_s/g_1) A_a(s) A_r(s-f) / A_T(s), \quad (1c)$$

$T_e$  is the electron temperature, and  $n_e$  and  $n_1$  represent, respectively, the electron density and the ground-state density of the recombining ion. The total transition probability of the autoionizing state is  $A_T(s)$ ;  $A_a(s)$  and  $A_r(s-f)$  designate, respectively, the autoionization transi-

tion probability to the ground state and radiative transition probability of  $|s\rangle$  to the final state  $|f\rangle$ .  $g_s$  and  $g_f$  are the statistical weights of the autoionizing state and the ground state, respectively.  $E_s$  is the Auger electron energy.

The intensity of the resonance line,  $I_r$ , is given by

$$I_r = n_e n_1 C(1 + RC_r/C), \quad (2)$$

where the rate coefficient for production of the resonance line by electron excitation of the recombining ion in the ground state is designated by  $C$ . The radiative capture rate coefficient of an ion with one less electron than the recombining ion is  $C_r$ , and  $R$  represents the ratio of density of the ion with one less electron than the recombining ion and  $n_1$ . Both these rate coefficients depend on the electron temperature.

The total dielectronic recombination rate  $\alpha_d$  is given by

$$\alpha_d = \sum_i \alpha_d(i-f) + \sum_i \alpha_d(i-s) A_r(s-f)/A_r(s), \quad (3)$$

where the second term represents contributions from cascades.

### B. Transition rates

The x-ray transition rates  $A_x$  for spontaneous emission of a photon of energy  $c\hbar k$  is<sup>26</sup>

$$A_x(SLJ-S'L'J') = \frac{4k^3}{3\hbar} \frac{1}{2J+1} |\langle \gamma'S'L'J' | |D| | \gamma SLJ \rangle|^2,$$

where  $| \gamma SLJ \rangle$  and  $| \gamma'S'L'J' \rangle$  represent the initial and final states of the system, respectively,  $D$  is the electric dipole operator,  $\langle \gamma'L'J' | |D| | \gamma LJ \rangle$  is the reduced matrix element, and  $\gamma$  represents any additional quantum numbers that may be needed to specify the atomic state functions uniquely. For transition of satellite lines of the type  $|2p nl SLJM\rangle$  to  $|1s nl SL'J'M'\rangle$ , the reduced matrix element is

$$\begin{aligned} & \langle 1s nl S'L'J' | |D| | 2p nl SLJ \rangle \\ &= (-1)^{S+L+J'+1} [(2J+1)(2J'+1)]^{1/2} \\ & \times \begin{Bmatrix} J' & 1 & J \\ L & S & L' \end{Bmatrix} I(2p-1s) [(2L+1)/3]^{1/2}, \end{aligned}$$

where

$$I(2p-1s) = e \int R(2p,r)rR(1s,r)r^2 dr.$$

The autoionization transition rate is given by

$$A_a(\gamma SLJ) = (2\pi/\hbar) |\langle \gamma'S'L'J' | V | \gamma SLJ \rangle|^2,$$

where

$$V = \sum_{\substack{i,j \\ (i>j)}} (1/r_{ij})$$

is the two-electron interaction operator, and the continuum electron orbital has been normalized per unit energy. For the transition  $n_1 l_1 n_2 l_2 - n_0 l_0 l_c$  we obtain the matrix element

$$\begin{aligned} & \langle \gamma'S'L'J' | V | \gamma SLJ \rangle \\ &= \sum_k [a_k R^k(l_1 l_2; l_0 l_c) + b_k R^k(l_1 l_2; l_c l_0)] \delta_{JJ'}, \end{aligned}$$

where

$$\begin{aligned} a_k &= (-1)^p [(2l_1+1)(2l_2+1)(2l_0+1)(2l_c+1)]^{1/2} \\ & \times \begin{Bmatrix} l_1 & l_2 & L \\ l_c & l_0 & k \end{Bmatrix} \begin{Bmatrix} l_1 & k & l_0 \\ 0 & 0 & 0 \end{Bmatrix} \begin{Bmatrix} l_2 & k & l_c \\ 0 & 0 & 0 \end{Bmatrix}, \end{aligned}$$

$$p = l_1 + l_0 + L,$$

$$\begin{aligned} b_k &= (-1)^q [(2l_1+1)(2l_2+1)(2l_0+1)(2l_c+1)]^{1/2} \\ & \times \begin{Bmatrix} l_1 & l_2 & L \\ l_0 & l_c & k \end{Bmatrix} \begin{Bmatrix} l_1 & k & l_c \\ 0 & 0 & 0 \end{Bmatrix} \begin{Bmatrix} l_2 & k & l_0 \\ 0 & 0 & 0 \end{Bmatrix}, \end{aligned}$$

and

$$q = l_1 + l_0 + S.$$

### III. NUMERICAL CALCULATIONS

The radial one-electron orbitals were generated using the nonrelativistic Hartree-Fock-Slater atomic model.<sup>27</sup> Uncorrelated configuration state functions (CSF)  $\phi(\gamma SLJ)$  were obtained by usual angular momentum coupling. Atomic state functions (ASF)

$$\psi_i = \sum_j C_{ij} \phi_j(\gamma SLJ)$$

were then constructed as a superposition of CSF's. The mixing coefficients  $C_{ij}$  were determined by solving the set of  $N$  simultaneous linear homogeneous equations

$$\sum_{k=1}^N \langle \phi_i | H | \phi_k \rangle C_{jk} = E_j C_{ij}$$

subject to the condition

$$\sum_k C_{ik}^* C_{jk} = \delta_{ij} \quad (i, j = 1, 2, \dots, N),$$

where  $E_i$  is the energy corresponding to the ASF  $\psi_i$ , and  $N$  is the dimension of the energy matrix. These ASF's are then used to calculate the transition matrix elements of Sec. II. The diagonal terms  $\langle \phi_i | H | \phi_i \rangle$  were corrected for relativistic effects through perturbation using uncorrelated CFS's as the basis. For a few prominent satellite lines, x-ray wavelengths are calculated relativistically including radiative corrections of quantum electrodynamics.

### IV. RESULTS AND DISCUSSIONS

#### A. Wavelengths, transition rates, and $F_2$ functions

Table I contains x-ray wavelengths, Auger and radiative decay rates, and  $F_2^*$  functions for the  $2l2l'$  complex. Wavelengths and transition rates calculated by Vainshtein and Safronova<sup>17</sup> using the  $Z$ -expansion technique are also listed for comparison. The largest discrepancy in wavelengths between the present HFS calculation (with relativistic corrections) and of Vainshtein and Safronova is 0.0010 Å for the transition  $2s2p^1P_1 - 1s2s^1S_0$ . In all

TABLE I. X-ray wavelengths  $\lambda$  (in Å), radiative decay rates  $A_r(s-f)$ , autoionization rates  $A_a(s)$ , total x-ray rate  $\sum_i A_r(s-i)$  and  $F_2^*(s-f)$  for  $2l2l'$  states of He-like chromium. Transition rates and  $F_2^*$  values are in units of  $10^{13} \text{ s}^{-1}$ . The first line in each case lists HFS values, followed by the Z-expansion values. Lines with  $F_2^*$  values less than  $10^{12} \text{ s}^{-1}$  are not listed.

Upper state $ s\rangle$	Final state $ f\rangle$	$\lambda$	$\lambda$ (MCDF)	$A_r(s-f)$	$A_a(s)$	$\sum_i A_r(s-i)$	$F_2^*(s-f)$
$2s2p(^1P_1)$	$1s2s(^3S_1)$	2.0899	2.0907	0.46	18.62	20.16	0.33
		2.0905		0.54	19.70	20.24	0.40
$2p^2(^1S_0)$	$1s2p(^1P_1)$	2.0952	2.1179	35.82	3.33	35.83	1.52
		2.0952		35.20	3.41	35.30	1.55
$2s2p(^1P_1)$	$1s2s(^1S_0)$	2.0997	2.1014	19.70	18.62	20.16	14.19
		2.1007		20.30	19.7	20.3	15.00
$2p^2(^1D_2)$	$1s2p(^3P_2)$	2.1007	2.1014	6.98	28.15	41.07	7.09
		2.1010		7.85	27.9	41.18	7.93
$2s2p(^3P_2)$	$1s2s(^3S_1)$	2.1021	2.1029	20.08	1.37	20.08	3.21
		2.1022		20.5	1.35	20.5	3.17
$2p^2(^3P_2)$	$1s2p(^3P_1)$	2.1027	2.1036	11.93	8.16	41.06	4.95
		2.1031		12.2	9.46	40.99	5.72
$2s2p(^3P_1)$	$1s2s(^3S_1)$	2.1058	2.1069	19.53	1.76	19.97	2.38
		2.1061		19.9	1.84	20.42	2.47
$2p^2(^3P_2)$	$1s2p(^3P_2)$	2.1063	2.1073	23.86	8.16	41.06	9.89
		2.1066		22.9	9.46	40.99	10.73
$2p^2(^1D_2)$	$1s2p(^1P_1)$	2.1070	2.1075	34.06	28.15	41.07	34.63
		2.1070		33.3	27.9	41.15	33.63
$2p^2(^3P_0)$	$1s2p(^3P_1)$	2.1070	2.1082	38.57	0.26	38.99	0.13
		2.1074		38.10	0.31	38.68	0.15
$2s2p(^3P_0)$	$1s2s(^3S_1)$	2.1071	2.1082	19.94	1.37	19.94	0.64
		2.1074		20.40	1.35	20.40	0.63
$2p^2(^3P_2)$	$1s2p(^1P_1)$	2.1126	2.1134	5.26	8.16	41.06	2.18
		2.1127		5.89	9.46	40.99	2.76
$2s^2(^1S_0)$	$1s2p(^3P_1)$	2.1190	2.1196	2.39	31.39	7.57	0.96
		2.1190		2.71	32.40	7.76	1.09
$2s^2(^1S_0)$	$1s2p(^1P_1)$	2.1291	2.1296	5.18	31.39	7.57	2.07
		2.1288		5.05	32.40	7.76	2.04

other cases the difference is within 0.0006 Å.

Mohr<sup>28</sup> has reported energy levels of hydrogenlike atoms based on a complete nonperturbative numerical calculation. Wavelengths of Lyman- $\alpha_1$  and - $\alpha_2$  lines determined from these energy levels, which are expected to be accurate up to seven significant digits, are 2.090 144 and 2.095 567 Å, respectively. We have calculated wavelengths of Lyman  $\alpha_1(2p_{3/2}-1s_{1/2})$  and  $\alpha_2(2p_{1/2}-1s_{1/2})$  and a few prominent satellite lines relativistically including corrections from self-energy and vacuum polarization. Wavelengths of Lyman  $\alpha_1$  and  $\alpha_2$  were, respectively, 2.0901 and 2.0955 Å. The wavelengths calculated from multiconfiguration Dirac-Fock (MCDF) program with radiative corrections are systematically larger than the values from HFS calculation and of Vainshtein and Safronova by about 0.0004 to 0.0009 Å. This discrepancy can mainly be attributed to the Lamb shift of quantum electrodynamics. Total energies of  $1s2l'$  and  $2l2l'$  configurations change, respectively, by about 2.95 and 0.4 eV because of Lamb shift. This decreases the transition energy by about 2.5 eV, with a corresponding increase in wavelength of about 0.0009 Å.

Except for certain spin-forbidden lines, the radiative transition rates from the present calculation are within 2% of the rates reported by Vainshtein and Safronova.<sup>17</sup>

The disagreement is about 12% for those transitions involving a spin change. For similar transitions in heliumlike titanium and iron,<sup>8</sup> discrepancies as large as 25% and 18%, respectively, have been reported by Bitter *et al.*<sup>1</sup> between calculations, using the Z-expansion technique and the Thomas-Fermi model. The Auger transition rates differ in most cases by 3% from the rates of Vainshtein and Safronova. For the  $2p^2(^3P_2)$  state which cannot autoionize in pure LS coupling because of parity selection rule, the discrepancy is 16%. Autoionization rate for this state in heliumlike titanium obtained employing the Z-expansion technique and using the Thomas-Fermi model differ, for example, by 34%.<sup>1</sup> Our values of  $F_2^*$  for  $2l2l'$  configurations are in reasonable agreement (within 1–13%) with those of Vainshtein and Safronova.

X-ray wavelengths, radiative transition rates, and  $F_2^*$  functions for  $2l3l'$  and  $2l4l'$  configurations are listed in Table II. Auger-electron energies, Auger transition rates, lifetime, and nonradiative branching ratios are listed in Table III. A multitude of initial states result from angular momentum coupling; these states decay through many different radiative channels. To keep the length of the tables within reasonable limits, channels for which  $F_2^*$  functions are less than  $10^{12} \text{ sec}^{-1}$  and nonradiative branching ratio less than 1% are not included. A com-

TABLE II. X-ray wavelengths,  $\lambda$  (in Å), radiative decay rates  $A_r(s-f)$ , total radiative rates  $\sum_i A_r(s-i)$ , and  $F_2^*(s-f)$  for  $2l3l'$  and  $2l4l'$  states of He-like chromium. Transition rate and  $F_2^*$  values are in units of  $10^{13} \text{ s}^{-1}$ . The wavelength using MCDF atomic model including QED corrections are listed in parentheses for some cases. Lines with  $F_2^*$  values less than  $10^{12} \text{ s}^{-1}$  are not listed.

Upper state $ s\rangle$	Final state $ f\rangle$	$\lambda$	$A_r(s-f)$	$\sum_i A_r(s-i)$	$F_2^*(s-f)$
$2s3p(^3P_2)$	$1s2s(^3S_1)$	1.7829	4.42	7.98	0.69
$2s3p(^3P_1)$	$1s2s(^3S_1)$	1.7837	3.97	8.96	0.52
$2p3s(^1P_1)$	$1s2s(^1S_0)$	1.7842	1.52	17.33	0.71
$2p3p(^3P_2)$	$1s2p(^3P_1)$	1.7846	2.84	24.05	0.11
$2p3p(^1D_2)$	$1s2p(^3P_2)$	1.7847	0.49	23.59	0.42
$2s3d(^1D_2)$	$1s2p(^3P_1)$	1.7862	0.93	8.54	0.53
$2p3p(^1S_0)$	$1s2p(^1P_1)$	1.7878	4.37	23.88	0.12
$2p3p(^3D_3)$	$1s2p(^3P_2)$	1.7879	4.17	20.76	0.10
$2p3p(^1D_2)$	$1s2p(^1P_1)$	1.7892	3.84	23.59	3.29
$2s3d(^3D_2)$	$1s2p(^3P_2)$	1.7898	1.10	8.57	0.29
$2s3s(^1S_0)$	$1s2p(^3P_1)$	1.7919	0.34	6.69	0.12
$2s3d(^1D_2)$	$1s2p(^1P_1)$	1.7934	0.65	8.54	0.37
$2s3d(^3D_2)$	$1s2p(^1P_1)$	1.7943	0.38	8.57	0.10
$2s3s(^1S_0)$	$1s2p(^1P_1)$	1.7991	0.89	6.69	0.32
$2p3d(^1F_3)$	$1s3d(^3D_2)$	2.0873	6.96	25.11	1.86
$2p3d(^1F_3)$	$1s3d(^3D_3)$	2.0877	2.13	25.11	0.57
$2p3d(^1F_3)$	$1s3d(^1D_2)$	2.0878	12.30	25.11	3.28
$2p3s(^1P_1)$	$1s3s(^3S_1)$	2.0879	1.61	17.33	0.75
$2p3p(^1S_0)$	$1s3p(^1P_1)$	2.0883	17.67	23.88	0.47
$2p3p(^1D_2)$	$1s3p(^3P_2)$	2.0885	1.32	23.59	1.13
		(2.0898)			
$2p3p(^1D_2)$	$1s3p(^1P_1)$	2.0901	16.14	23.59	13.82
		(2.0915)			
$2p3s(^1P_1)$	$1s3s(^1S_0)$	2.0904	12.13	17.33	5.65
$2p3d(^3D_3)$	$1s3d(^3D_2)$	2.0911	9.78	23.76	0.24
$2p3d(^3D_3)$	$1s3d(^3D_3)$	2.0915	10.48	23.76	0.25
$2p3d(^3P_2)$	$1s3d(^3D_1)$	2.0916	9.13	21.76	0.13
$2p3p(^3P_2)$	$1s3p(^3P_2)$	2.0920	17.69	24.05	0.67
		(2.0927)			
$2p3s(^3P_2)$	$1s3s(^3S_1)$	2.0924	15.82	20.94	0.25
$2p3p(^3D_3)$	$1s3p(^3P_2)$	2.0930	16.59	20.76	0.42
$2p3s(^1P_1)$	$1s3d(^3D_1)$	2.0931	1.22	17.33	0.57
$2p3d(^3F_4)$	$1s3d(^3D_3)$	2.0931	21.21	21.21	2.07
$2s3d(^1D_2)$	$1s3p(^3P_1)$	2.0932	0.21	8.54	0.12
$2s3d(^1D_2)$	$1s3p(^3P_2)$	2.0943	1.35	8.54	0.76
		(2.0948)			
$2s3d(^3d_2)$	$1s3p(^3P_1)$	2.0944	5.86	8.57	1.55
		(2.0953)			
$2p3d(^3P_1)$	$1s3d(^3d_1)$	2.0947	16.08	21.96	0.60
$2s3d(^3D_1)$	$1s3p(^3P_1)$	2.0947	7.28	10.51	0.16
$2p3s(^3P_1)$	$1s3s(^3S_1)$	2.0948	11.97	15.87	0.77
$2p3d(^1D_2)$	$1s3d(^1D_2)$	2.0958	9.12	20.45	0.14
$2s3d(^1D_2)$	$1s3p(^1P_1)$	2.0959	4.79	8.54	2.72
		(2.0964)			
$2p3d(^3F_3)$	$1s3d(^3D_2)$	2.0963	4.54	21.72	0.38
$2p3d(^3F_3)$	$1s3d(^1D_2)$	2.0968	7.96	21.72	0.66
$2p3d(^3F_3)$	$1s3d(^3D_3)$	2.0968	8.61	21.72	0.72
$2s3p(^3P_1)$	$1s3s(^3S_1)$	2.0968	3.57	8.96	0.47
$2s3d(^3D_3)$	$1s3p(^3P_2)$	2.0969	4.72	8.59	0.15
$2p3d(^3F_2)$	$1s3d(^3D_2)$	2.0969	16.44	22.18	0.37
$2p3s(^3P_0)$	$1s3s(^3S_1)$	2.0975	12.79	14.99	0.23
$2p3p(^3D_2)$	$1s3p(^3P_1)$	2.0977	14.51	21.30	0.72
		(2.0986)			
$2s3s(^1S_0)$	$1s3p(^3P_1)$	2.1009	1.42	6.69	0.50
$2s3p(^3P_2)$	$1s3d(^3D_3)$	2.1015	2.37	7.98	0.37
$2s3s(^1S_0)$	$1s3p(^1P_1)$	2.1037	3.48	6.69	1.23

TABLE II. (Continued).

Upper state $ s\rangle$	Final state $ f\rangle$	$\lambda$	$A_f(s-f)$	$\sum_i A_r(s-i)$	$F_2^*(s-f)$
$2s4p(^3P_2)$	$1s2s(^3S_1)$	1.6949	1.75	5.67	0.17
$2p4s(^3P_1)$	$1s2s(^3S_1)$	1.6952	1.62	4.84	0.21
$2p4p(^1D_2)$	$1s2p(^3P_2)$	1.6991	0.32	23.34	0.14
$2s4p(^3P_1)$	$1s2s(^1S_0)$	1.7006	0.93	10.75	0.15
$2p4p(^1D_2)$	$1s2p(^1P_1)$	1.7032	1.67	23.34	0.75
$2p4d(^1F_3)$	$1s4d(^3D_2)$	2.0887	1.23	22.88	0.19
$2p4d(^1F_3)$	$1s4d(^3D_3)$	2.0889	1.24	22.88	0.19
$2p4d(^1F_3)$	$1s4d(^1D_2)$	2.0890	19.06	22.88	2.95
$2p4f(^1D_2)$	$1s4f(^1F_3)$	2.0892	18.05	21.96	0.17
$2p4f(^1G_4)$	$1s4f(^3F_3)$	2.0893	16.61	21.93	0.14
$2p4s(^1P_1)$	$1s4s(^3S_1)$	2.0895	4.89	19.92	0.73
$2p4f(^3G_5)$	$1s4f(^3F_4)$	2.0895	21.55	21.96	0.15
$2p4p(^1D_2)$	$1s4p(^3P_2)$	2.0896	1.67	23.34	0.75
$2p4p(^1S_0)$	$1s4p(^1P_1)$	2.0899	16.27	22.93	0.24
$2p4p(^1D_2)$	$1s4p(^1P_1)$	2.0903	18.69	23.34	8.43
$2p4d(^1D_2)$	$1s4d(^3D_1)$	2.0904	9.73	21.69	0.11
$2p4d(^3D_3)$	$1s4d(^3D_3)$	2.0905	18.54	22.19	0.36
$2p4s(^1P_1)$	$1s4s(^1S_0)$	2.0906	14.46	19.92	2.16
$2p4d(^3F_4)$	$1s4d(^3D_3)$	2.0907	21.26	21.46	1.13
$2p4p(^3D_3)$	$1s4p(^3P_2)$	2.0909	20.93	23.28	0.16
$2p4p(^3P_2)$	$1s4p(^3P_2)$	2.0911	19.48	23.65	0.72
$2s4p(^3P_1)$	$1s4s(^3S_1)$	2.0941	7.95	10.75	1.29
$2s4d(^3D_2)$	$1s4p(^3P_1)$	2.0946	5.27	7.36	0.73
$2s4f(^3F_3)$	$1s4d(^3D_2)$	2.0946	3.49	4.55	0.19
$2s4d(^3D_1)$	$1s4p(^3P_1)$	2.0946	8.38	10.30	0.11
$2p4d(^3F_3)$	$1s4d(^3D_2)$	2.0954	14.81	16.95	0.66
$2p4d(^3D_2)$	$1s4d(^3D_2)$	2.0956	15.68	19.73	0.15
$2p4s(^3P_1)$	$1s4s(^3S_1)$	2.0957	1.12	4.84	0.14
$2p4p(^3D_2)$	$1s4p(^3P_1)$	2.0958	14.05	16.55	0.93
$2p4s(^3P_0)$	$1s4s(^3S_1)$	2.0961	11.49	12.64	0.10
$2s4p(^3P_2)$	$1s4d(^3D_3)$	2.0976	2.53	5.67	0.25
$2s4s(^1S_0)$	$1s4p(^3P_1)$	2.0976	2.27	6.25	0.57
$2p4s(^3P_1)$	$1s4d(^3D_1)$	2.0979	0.94	4.84	0.12
$2s4s(^1S_0)$	$1s4p(^1P_1)$	2.0987	3.14	6.25	0.79

plete listing for all transitions may be obtained from the authors.

The first few lines in Table II have wavelengths considerably shorter than the resonance lines. These are mostly correlation satellite lines and lines involving transitions  $2l3l'-1s2l$ . Existence of a few dielectronic satellite lines with wavelengths shorter than the Lyman- $\alpha_1$  and  $-\alpha_2$  lines suggests, however, that like the  $2l2l'$  configurations all these wavelengths are to be shifted to higher values. To estimate the magnitude of this shift, we have performed a MCDF calculation with radiative corrections for wavelengths of some of the satellite lines of the  $2l3l'$  complex. These are listed in parentheses in Table II. Wavelengths from the MCDF calculation for the selected transitions are 0.0005–0.0014 Å larger than the HFS values. As in the case of  $2l2l'$  configurations, about 0.0009 Å of this difference may be attributed to Lamb shift.

In Table IV we list x-ray wavelengths, radiative transition rates, and fluorescence yields for all states with fluorescence yield greater than 80%. These represent the prominent lines on the x-ray spectrum for deexcitation of prepared doubly excited states of heliumlike chromium.

Such is approximately the case for spectra obtained in ion-atom collision experiments. Transition from  $2l2l'$  configurations produces x rays of wavelengths between 2.095 and 2.130 Å, while Auger transitions contribute between 4024 and 4119 eV. Nonradiative transition from  $2s^2(^1S_0)$  at 4024.7 eV,  $2s2p(^1P_1)$  at 4078 eV, and  $2p^2(^1D_2)$  at 4086 eV constitute the most prominent Auger lines. The state  $2s^2(^1S_0)$  cannot ordinarily decay by the electric dipole transition, it picks up strength from configuration mixing and decays by E1 emission with a fluorescence yield of 19.5%. X-ray transitions  $2p^2(^3P_0)-1s2p(^3P_1)$ ,  $2p^2(^1S_0)-1s2p(^1P_1)$ ,  $2s2p(^3P_0)-1s2s(^3S_1)$ , and  $2s2p(^3P_2)-1s2s(^3S_1)$  have, respectively, fluorescence yields of 98%, 91%, 94%, and 94%, and constitute the strongest x-ray lines of  $2l2l'$  configurations. For dielectronic satellite lines, however, it is the  $F_2$  functions and not the fluorescence yield that determines the strength of a line. The transition  $2p^2(^1D_2)-1s2p(^1P_1)$ ,  $2s2p(^1P_1)-1s2s(^1S_0)$ , and  $2p^2(^3P_2)-1s2p(^3P_2)$  with  $F_2$  functions 34.6, 14.2, and 9.9, respectively, are the strongest satellite lines. Transitions from  $2l3l'$  and  $2l4l'$  configurations produce Auger lines between 5092.8 and 5138.5 eV, and

TABLE III. Auger-electron energies (in eV), lifetimes [ $1/A_T(s)$ ], autoionization transition rates, and Auger yields [ $A_a(s)/A_T(s)$ ] for doubly excited heliumlike chromium. Lifetimes and transition rates are in units of  $10^{-15}$  s and  $10^{13}$  s $^{-1}$ , respectively. Transitions for which Auger yield is less than 1% are not listed.

Autoionizing state $ s\rangle$	Auger energy	Lifetime	$A_a(s)$	Auger yield
$2s^2(^1S_0)$	4024.7	2.5665	31.39	80.6
$2p^2(^1S_0)$	4119.1	2.5533	3.33	8.5
$2p^2(^3P_2)$	4070.2	2.0316	8.16	16.6
$2p^2(^1D_2)$	4086.0	1.4447	28.15	40.7
$2s2p(^1P_1)$	4078.1	2.5785	18.62	48.0
$2s2p(^3P_0)$	4029.7	4.6925	1.37	6.4
$2s2p(^3P_1)$	4033.4	4.6006	1.76	8.1
$2s2p(^3P_2)$	4043.7	4.6612	1.37	6.4
$2s3s(^1S_0)$	5092.8	4.3879	16.10	70.7
$2s3p(^3P_1)$	5096.8	10.1812	0.86	8.8
$2s3p(^3P_2)$	5099.6	11.7435	0.53	6.2
$2s3d(^1D_2)$	5114.7	9.0565	2.50	22.7
$2s3d(^3D_1)$	5110.5	9.3735	0.16	1.5
$2s3d(^3D_2)$	5111.4	10.4286	1.01	10.6
$2p3s(^1P_1)$	5122.0	3.9781	7.81	31.0
$2p3s(^3P_0)$	5094.9	6.4282	0.57	3.7
$2p3s(^3P_1)$	5102.5	6.0301	0.71	4.3
$2p3p(^1S_0)$	5136.5	3.9650	1.34	5.3
$2p3p(^1D_2)$	5131.2	2.7873	12.29	34.2
$2p3p(^3D_2)$	5101.9	4.6018	0.43	2.0
$2p3d(^3P_1)$	5117.4	4.4411	0.56	2.5
$2p3d(^1F_3)$	5138.5	3.6785	2.07	7.6
$2p3d(^3F_3)$	5113.0	4.4948	0.53	2.3
$2p3d(^3F_4)$	5123.3	4.6118	0.47	2.2
$2s4s(^1S_0)$	5457.2	7.9951	6.26	50.0
$2s4p(^3P_1)$	5463.9	8.2895	1.31	10.8
$2s4p(^3P_2)$	5460.6	16.9270	0.23	3.9
$2s4d(^3D_2)$	5465.6	12.8332	0.43	5.5
$2s4d(^3D_3)$	5464.6	39.1176	0.08	3.0
$2s4f(^1F_3)$	5468.8	73.8407	0.01	1.1
$2s4f(^3F_3)$	5468.4	21.6557	0.07	1.6
$2p4s(^1P_1)$	5476.7	4.5215	2.20	9.9
$2p4s(^3P_0)$	5458.2	7.7694	0.23	1.8
$2p4s(^3P_1)$	5459.3	18.8885	0.45	8.6
$2p4p(^1S_0)$	5482.3	4.2323	0.70	3.0
$2p4p(^1D_2)$	5481.1	3.5112	5.14	18.0
$2p4p(^3D_2)$	5462.1	5.8832	0.45	2.7
$2p4d(^1F_3)$	5485.2	4.1764	1.06	4.4
$2p4d(^3F_3)$	5466.4	5.8249	0.22	1.3
$2p4d(^3F_4)$	5480.0	4.6037	0.26	1.2

between 5457.2 and 5485.2 eV, respectively. The prominent dielectronic satellite lines from these configurations are  $2p3p(^1D_2)$ - $1s3p(^1P_1)$ ,  $2p4p(^1D_2)$ - $1s4p(^1P_1)$ , and  $2p3s(^1P_1)$ - $1s3s(^1S_0)$ , with  $F_2^*$  values 13.8, 8.4, and 5.6, respectively.

#### B. Dielectronic recombination and temperature diagnostic

Satellite lines in the vicinity of the resonance Lyman- $\alpha$  lines are due to transition  $1snl$ - $2pnl$ . These doubly excited

TABLE IV. X-ray wavelengths,  $\lambda$  in  $\text{\AA}$ , radiative transition rate  $A_r(s-f)$  in units of  $10^{13}$  s $^{-1}$ , and level fluorescence yield  $\omega = A_r(s-f)/A_T(s)$  for  $2lnl'$  electron configurations of  $\text{Cr}^{22+}$ . Only transitions with  $\omega \geq 0.8$  are listed.

Upper state $ s\rangle$	Final state $ f\rangle$	$\lambda$	$A_r(s-f)$	$100\omega$
$2p_2(^1S_0)$	$1s2p(^1P_1)$	2.0952	35.82	91.47
$2p_2(^3P_0)$	$1s2p(^3P_1)$	2.1070	38.57	98.24
$2s2p(^3P_0)$	$1s2s(^3S_1)$	2.1071	19.94	93.57
$2s2p(^3P_1)$	$1s2s(^3S_1)$	2.1058	19.53	89.86
$2s2p(^3P_2)$	$1s2s(^3S_1)$	2.1021	20.08	93.61
$2p3s(^3P_0)$	$1s3s(^3S_1)$	2.0975	12.79	82.23
$2p3d(^3P_0)$	$1s3d(^3D_1)$	2.0897	20.08	90.13
$2p3d(^3F_4)$	$1s3d(^3D_3)$	2.0931	21.21	97.83
$2s4p(^3P_0)$	$1s4s(^3S_1)$	2.0950	9.71	85.32
$2s4d(^3D_1)$	$1s4p(^3P_1)$	2.0946	8.38	80.72
$2p4s(^3P_0)$	$1s4s(^3S_1)$	2.0961	11.49	89.24
$2p4s(^3P_2)$	$1s4s(^3S_1)$	2.0902	20.04	94.57
$2p4p(^3P_2)$	$1s4p(^3P_2)$	2.0911	19.48	81.16
$2p4p(^3D_2)$	$1s4p(^3P_1)$	2.0958	14.05	82.67
$2p4p(^3D_3)$	$1s4p(^3P_2)$	2.0909	20.93	89.71
$2p4d(^3P_0)$	$1s4d(^3D_1)$	2.0897	20.98	95.95
$2p4d(^3D_3)$	$1s4d(^3D_3)$	2.0905	18.54	83.11
$2p4d(^3F_3)$	$1s4d(^3D_2)$	2.0954	14.81	86.27
$2p4d(^3F_4)$	$1s4d(^3D_3)$	2.0907	21.26	97.88
$2p4f(^1D_2)$	$1s4f(^1F_3)$	2.0892	18.05	81.91
$2p4f(^3D_1)$	$1s4f(^3F_2)$	2.0892	21.49	98.11
$2p4f(^3F_3)$	$1s4f(^3F_3)$	2.0949	17.43	80.26
$2p4f(^3G_5)$	$1s4f(^3F_4)$	2.0895	21.55	98.01

He-like states can be produced only by dielectronic recombination since the electron excitation cannot populate these states. The intensity ratio of  $I_d(s-f)$  and  $I_r$  depend primarily on the electron temperature. The contribution of radiative electron capture in Eq. (12) is negligible for medium atomic numbers in high-temperature plasmas. Contributions of unresolved dielectronic satellite lines that merge with resonance line to the experimental intensity of the resonance line can best be calculated by constructing a synthetic spectrum<sup>1</sup> using the theoretical values of  $F_2^*$ . However, these effects can be approximated for states with large  $n$  values by adding

$$C_D \equiv \sum_i \alpha_d(i-f)/C$$

to the term in the parentheses of Eq. (2). The contribution to the dielectronic satellites by cascade from higher-lying autoionizing states can be taken into account by multiplying the right-hand of Eq. (1a) by

$$C_{\text{cas}} = 1 + \sum_i \alpha_d(i-s)/\alpha_d(s-f)A_x(s-f)/A_T(s).$$

The values of  $C_{\text{cas}}$  range from 1.006 to 1.05 for the strong dielectronic satellite lines at  $kT_e \approx 3$  keV.

Total dielectronic recombination (DR) rate coefficient for hydrogenlike chromium is plotted in Fig. 1 as a function of electron temperature. The contributions to the DR rate coefficient from  $2lnl'$  configurations decrease as  $n$  in-

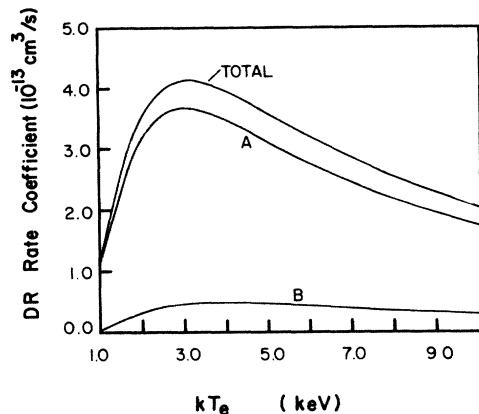


FIG. 1. Total dielectronic recombination (DR) rate coefficients vs  $kT_e$  where  $T_e$  is the electron temperature. The curve *A* gives sum of partial DR rate coefficients for  $2lnl'$ ,  $n=2, 3$ , and 4 while curve *B* is the sum of contributions from all other channels with  $n \geq 5$ .

creases; the contribution of  $n \geq 5$  is approximately 12% at  $kT_e = 3$  keV. Average configuration rates were used for  $n=5-8$ , and  $1/n^3$  scaling was employed for  $n > 8$ . The maximum value of  $\alpha_d$  is  $4.1 \times 10^{13} \text{ cm}^3 \text{ s}^{-1}$  at  $kT_e \approx 3$  keV. Corresponding values for hydrogenlike titanium<sup>1</sup>

are  $3.6 \times 10^{13} \text{ cm}^3 \text{ s}^{-1}$  with the TF model and  $4.3 \times 10^{13} \text{ cm}^3 \text{ s}^{-1}$  with the *Z*-expansion method.

## V. CONCLUSIONS

We have presented the results of our extensive calculations for doubly excited He-like chromium for states with  $2lnl'$  configurations for  $n=2, 3$ , and 4. The atomic parameters needed for obtaining the wavelengths and intensities of dielectronic satellite lines of the H-like chromium are presented. The importance of cascade contributions to dielectronic satellite lines and contribution of unresolved lines to resonance lines are discussed. Our results of  $F_2^*$  agree within a range of 1–13% with the values obtained with the *Z*-expansion technique for  $2l2l'$  configurations. The HFS wavelengths are in excellent agreement with the corresponding values with the *Z*-expansion method. Wavelengths of a few strong dielectronic satellite lines are also presented using the relativistic multiconfiguration Dirac-Fock model and the QED correction were included by perturbation theory.

## ACKNOWLEDGMENTS

This work was supported by the Division of Chemical Science, Office of Basic Energy Science, Office of Energy Research, and U.S. Department of Energy.

<sup>1</sup>M. Bitter, S. von Goeler, S. Cohen, K. W. Hill, S. Sesnic, F. Tenney, J. Timberlake, U. I. Safronova, L. A. Vainshtein, J. Dubau, M. Loulergue, F. Bely-Dubau, and L. Steenman-Clark, *Phys. Rev. A* **29**, 661 (1984).

<sup>2</sup>TFR Group, F. Bombarda, F. Bely-Dubau, P. Faucher, M. Cornille, J. Dubau, and M. Loulergue, *Phys. Rev. A* **32**, 2374 (1985); TFR Group, M. Cornille, J. Dubau, and M. Loulergue, *ibid.* **32**, 3000 (1985).

<sup>3</sup>E. Källne, J. Källner, E. S. Marmar, and J. G. Rice, *Phys. Scr.* **31**, 551 (1985); E. Källne, J. Källne, and J. E. Rice, *Phys. Rev. Lett.* **49**, 330 (1982).

<sup>4</sup>E. V. Aglizki, V. A. Boiko, A. Ya Faenov, V. V. Korneev, V. V. Krutov, S. L. Mandelstam, S. A. Pikuz, U. I. Safronova, J. A. Sylvester, A. M. Urinov, A. M. Vainshtein, and L. A. Zhitnik, *Solar Phys.* **56**, 375 (1978); J. H. Parkinson, R. S. Wolff, H. L. Kestenbaum, W. H. M. Ku, J. R. Lemen, K. S. Long, R. Novick, R. J. Suozzo, and M. C. Weisskopf, *ibid.* **60**, 123 (1978).

<sup>5</sup>G. A. Doschek, U. Feldman, and R. W. Kreplin, *Astrophys. J.* **239**, 725 (1980); **233**, L157 (1979).

<sup>6</sup>J. Dubau, M. Loulergue, and L. Steenman-Clark, *Mon. Not. R. Astron. Soc.* **190**, 125 (1980).

<sup>7</sup>A. N. Parmer, J. L. Culhane, C. G. Rapley, E. Antonucci, A. H. Gabriel, and M. Loulergue, *Mon. Not. R. Astron. Soc.* **197**, 29 (1981).

<sup>8</sup>J. Dubau, A. H. Gabriel, M. Loulergue, L. Steenman-Clark, and S. Volonte, *Mon. Not. R. Astron. Soc.* **195**, 705 (1981).

<sup>9</sup>K. Tanaka, T. Watanabe, K. Nishi, and K. Akita, *Astrophys. J.* **254**, L59 (1982).

<sup>10</sup>L. Blanchet, M. Cornille, J. Dubau, P. Faucher, J. Lion, and S. Volonte, *Astron. Astrophys.* **152**, 417 (1985).

<sup>11</sup>B. Yaakobi, D. Steel, E. Thorsos, A. Hauer, and B. Perry, *Phys. Rev. Lett.* **39**, 1526 (1977).

<sup>12</sup>J. F. Seely, *Phys. Rev. Lett.* **42**, 1606 (1979).

<sup>13</sup>K. B. Mitchell, D. B. VanHusteyn, G. H. McCall, P. Lee, and H. R. Griem, *Phys. Rev. Lett.* **42**, 232 (1979).

<sup>14</sup>J. M. Banon, M. Koenig, and H. Nguyen, *J. Phys. B* **4**, 4195 (1985).

<sup>15</sup>A. H. Gabriel, *Mon. Not. R. Astron. Soc.* **160**, 99 (1972); C. P. Bhalla, A. H. Gabriel, and L. P. Presnyakov, *ibid.* **172**, 359 (1975).

<sup>16</sup>For a review of the subject and references to earlier work, see J. Dubau and S. Volonté, *Rep. Prog. Phys.* **43**, 199 (1980).

<sup>17</sup>L. A. Vainshtein and U. I. Safronova, *At. Data Nucl. Data Tables* **21**, 49 (1978).

<sup>18</sup>M. Bitter (private communication).

<sup>19</sup>S. von Goeler, M. Bitter, S. Cohen, D. Eames, K. Hill, D. Hills, R. Hulse, G. Lenner, D. Manos, Ph. Roney, W. Roney, N. Sauthoff, S. Sesnic, W. Stodwick, F. Tenney, and J. Timberlake, in *Diagnostics for Fusion Reactor Conditions*, Proceedings of the International School of Plasma Physics, edited by P. E. Stott, D. K. Akulina, G. G. Leotta, E. Sindoni, and C. Wharton (Pergamon, New York, 1982), Vol. I, p. 109.

<sup>20</sup>T. Ohkawa, in *Physics of Plasmas Close to Thermonuclear Condition*, Proceedings of the International School of Plasma Physics, edited by B. Coppi, G. G. Leotta, D. Pfirsch, R. Pozzoli, and E. Sindoni (Pergamon, New York, 1981), Vol. II, p. 617.

<sup>21</sup>R. D. Bleach, P. G. Burkhalter, D. J. Nagel, and W. Rowan, in *Diagnostics for Fusion Reactor Condition*, Proceedings of the International School of Plasma Physics, edited by P. E.

- Stott, D. K. Akulina, G. G. Leotta, E. Sindoni, and C. Whar-  
ton (Pergamon, New York, 1982), Vol. II, p. 107.
- <sup>22</sup>TFR group, J. Dubau, and M. Loulergue, *J. Phys. B* **15**, 1007  
(1981).
- <sup>23</sup>W. Eissner, M. Jones, and H. Nussbaumer, *Comput. Phys.*  
*Commun.* **8**, 270 (1974).
- <sup>24</sup>C. P. Bhalla and K. R. Karim, *Nucl. Instrum. Methods* **57**,  
2055 (1986).
- <sup>25</sup>A. Burgess, *Astrophys. J.* **141**, 1588 (1965); Bruce W. Shore,  
*ibid.* **158**, 1205 (1969).
- <sup>26</sup>B. W. Shore and D. H. Manzel, *Principles of Atomic Spectra*  
(Wiley, New York, 1968); K. R. Karim, M. H. Chen, and B.  
Crasemann, *Phys. Rev. A* **29**, 2605 (1984).
- <sup>27</sup>C. P. Bhalla, N. O. Folland, and M. A. Hein, *Phys. Rev. A* **8**,  
649 (1973).
- <sup>28</sup>P. Mohr, *At. Data Nucl. Data Tables* **29**, 453 (1983).